Peer-Reviewed Technical Communication

A Small Autonomous Surface Vehicle for Ocean Color Remote Sensing

Elgar Desa, *Member, IEEE*, Pramod Kumar Maurya, Arvind Pereira, António M. Pascoal, R. G. Prabhudesai, Antonio Mascarenhas, Ehrlich Desa, R. Madhan, S. G. P. Matondkar, Gajanan Navelkar, Shivanand Prabhudesai, and Sanjeev Afzulpurkar

***Abstract*—This paper provides a study on the development and the use of a small autonomous surface vehicle (ASV) that automatically follows programmed mission transects, while measuring sensor outputs along the tracks. It discusses the mechanical construction of the ASV, the distributed architecture of controller area network (CAN)-based nodes for science and vehicle payloads, high-speed radio-frequency (RF) communications, the performance of the heading autopilot, global positioning system (GPS)-based guidance algorithm, and the mission programming technique. The field trials of the ASV, performed off the coast of Goa, India, are focused on retrieving the 2-D spatial distribution of surface chlorophyll, which is one of the useful parameters in characterizing the nature of calibration–validation (CALVAL) sites for ocean remote sensing needs. A further benefit of ASVs is that they can be built at a low cost and used in monitoring applications of diverse coastal ecosystems.**

***Index Terms*—Autonomous surface vehicles (ASVs), calibration–validation (CALVAL) sites, chlorophyll measurements, controller area network (CAN) nodes, mission control (MC), ocean remote sensing, vehicle control.**

I. Introduction

THE advent of ocean satellites with sensors to measure oceanic parameters of wind-induced waves, sea ice cover, precipitation, rainfall, ocean color, and sea surface temperature has made synoptic monitoring of large tracts of the ocean at a low cost a reality. For example, it has been estimated that the World Ocean Circulation Experiment (WOCE) data set from ships over several years can be repeated for less than 10% of its present cost by satellite observation [1]. In the context of this paper, operational ocean color satellites of the past, namely, the coastal zone color scanner (CZCS) and the present, namely, sea-viewing wide field-of-view sensor (SeaWiFs), moderate resolution imaging spectroradiometer (MODIS), OCEANSAT 1, and others, have generated large valuable data sets on chlorophyll distributions of open and coastal waters of different oceanic regimes. The benefits of this when combined with sea surface temperature enable the tracking of oceanic fronts and thus the prediction of potential fishing zones, and more refined models of primary production. However, it is still necessary to improve the quality of all remote sensed data by establishing well-located sea truth sites that can be used to calibrate and validate space sensors in orbit. Examples of known calibration–validation (CALVAL) sites are the Moby Optical Buoy off the Hawaiian Island of Lunai, which has been used in the vicarious calibration of the SeaWiFs ocean color satellite sensor, the Hawaiian ocean time series (HOTS), and the Bermuda Atlantic time series (BATS) sites used in providing standard references of remote sensing reflectance and chlorophyll concentrations for the MODIS color sensor. The Indian Space Research Organization (ISRO, Bangalore, India) which builds and launches ocean color satellite sensors is also in the process of establishing satellite transmitting CALVAL sites off the Lakswadeep Islands, and the Andaman and Nicobar Islands, India, to calibrate color satellite series OCEANSAT 1 and II.

Apart from absolute radiometric references, CALVAL sites can be used in validating and fine-tuning bio-optical algorithms for the retrieval of seawater constituents in coastal waters. In most cases, autonomous data logging systems on CALVAL buoys are programmed to log hyperspectral upward radiance from the sea surface, *in situ* chlorophyll, conductivity–temperature–depth (CTD), and meteorological parameters at programmed time intervals, and periodically transmit such data via satellite to a central receiving station on land. These systems are designed to operate around the year, except at times when the buoy is checked for maintenance or upgrades. As the buoy is fixed to a mooring, all data is referenced to a single point on the ocean corresponding to a single satellite pixel. An extension of this idea is the use of small autonomous surface vehicles (ASVs) fitted with optical payloads namely fluorometer, spectroradiometers, absorption meters, and meteorological sensors that can provide seasonal coverage, in principle, over several tens of satellite pixels around the CALVAL site. The resultant high-resolution spatial surface distributions from ASVs will complement CALVAL buoy data over a much wider area, thus enabling finer analytical insights into deciphering satellite received signals, and a better understanding of the statistical variability of oceanic parameters near a CALVAL site.

Manuscript received November 29, 2005; revised September 29, 2006; accepted December 15, 2006. This work was supported by the National Institute of Oceanography, Goa, India, under Millennium Projects.

Associate Editor: D. R. Blidberg.

E. Desa, P. K. Maurya, A. Pereira, R. G. Prabhudesai, A. Mascarenhas, R. Madhan, S. G. P. Matondkar, G. Navelkar, S. Prabhudesai, and S. Afzulpurkar are with the National Institute of Oceanography, Marine Instrumentation, Dona Paula, Goa 403004, India (e-mail: elgar@nio.org).

A. M. Pascoal is with the National Institute of Oceanography, Marine Instrumentation, Dona Paula, Goa 403004, India and also with the Instituto Superior Técnico—Institute of Systems and Robotics (IST-ISR), Lisbon 1049-001, Portugal (e-mail: antonio@isr.ist.utl.pt).

E. Desa is with the National Institute of Oceanography, Marine Instrumentation, Dona Paula, Goa 403004, India and also with the IOC UNESCO, Paris, France (e-mail: E.desa@unesco.org).

Color versions of one or more of the figures in this paper are available online at http://ieeexplore.ieee.org.

Digital Object Identifier 10.1109/JOE.2007.893688

ASVs are closely related to the family of autonomous underwater vehicles (AUVs). They are designed to navigate autonomously along programmed transects on the sea surface, holding course with high accuracy in the face of sea currents and wind. ASVs are not designed to dive below the sea surface, and are, therefore, much simpler data platforms to design and construct than AUVs. There are several examples of ASVs being developed for coastal applications. Noteworthy ASVs are the Delfim developed by the Institute of Systems and Robotics (ISR) of Instituto Superior Técnico (IST), Lisbon, Portugal [2] and the Autocat from AUV Laboratory, Massachusetts Institute of Technology (MIT, Cambridge, MA), which has been developing surface robot crafts since 1993 [3].

The Delfim is a small autonomous catamaran that measures 3.5 m long and 2.0 m wide, and weighs about 340 kg. Propulsion of the craft is done by two electric thrusters at a top speed of 5 kn. Two separate banks of onboard lead acid batteries, each with 3960-Wh energy, supply power to the craft. Vehicle navigation on Delfim relies on a high-precision differential global positioning system (DGPS), a Doppler unit, and a heading sensor. Delfim communicates with remote stations either on shore or to a support ship to receive commands and real-time global positioning system (GPS) corrections, and to send back status information as well as real-time data. An off-the-shelf 115 kBd radio modem is used as the radio-frequency (RF) link to the support ship. The Delfim catamaran has been deployed chiefly in bathymetric mapping surveys of seamounts and coastal areas in the Azores Islands, Portugal.

The Autocat is a much smaller catamaran with a length of 1.8 m, beam of 1 m, and a displacement of $\sim$100 kg. Navigation is done by DGPS with $<$3-m accuracy, with a speed range between 1 and 8 kn. The power sources on the catamaran are sealed lead acid batteries, and propulsion is done by direct current (dc) trolling motors. Autocat has been equipped with a subbottom profiler to survey buried shipwrecks, and has been used in defense surveys.

A third interesting development is the mobile unmanned surface vehicle, the Kan-Chan, built in 2000 by Yamaha Motor Company, Ltd. (Iwata, Shizuoka, Japan), in support of studies on global warming. The Kan-Chan hull design is based on the concept of a sailing cruiser with excellent course holding characteristics, a cruising speed of 4 kn in calm waters, and a continuous operating time of 700 h. A low center of gravity provides for quick righting capability. The vehicle is a large ASV having a total length of 8 m, a width of 2.8 m, and a displacement of 3500 kg. It is powered by a diesel engine, and employs a wind turbine generator for backup power.

At the National Institute of Oceanography, Goa, India, research and development efforts in the area of marine technology have led to the development of an ASV named remotely operable sea skimmer (ROSS) which as an early prototype could be operated remotely with a joystick, and as described here, as a complete autonomous vehicle. ROSS is a small craft having a length of 1.6 m, hull width of 35 cm, and a weight of 90 kg and it has two spaced out dc motors attached to its undercarriage (see Figs. 1 and 2). A change in heading of the craft is generated by application of a differential torque between the motors.

The original concept of ROSS arose from the need to collect additional oceanographic data when a research vessel halts at a station. We argued that for typical waiting periods of an hour or more, small mobile intelligent craft fitted with an appropriate suite of sensors could be deployed from the ship to sample and store and transmit oceanic surface properties, namely, the light field, chlorophyll, and temperature in the space surrounding the research vessel. The design of ROSS was unusual in that the main hull was partially submerged below the water line and propelled by two underwater dc motors [4].

Fig. 1. ROSS ASV.

The mechanical design of ROSS and its specifications are examined in Section II, followed by a description of the method used here in calibrating the *in situ* chlorophyll sensor (Section III). The distributed electronic architecture of controller area network (CAN) nodes used in controlling ROSS is covered in Section IV. ROSS maintains contact over a high-speed RF link with the shore/ship-based user who can instruct it to execute a mission control (MC) program (Sections V and VI). A vehicle model is derived from open-loop responses, and used in the simulation and in setting the gains of the heading autopilot (Section VII). GPS-assisted navigation and guidance using a conventional line-of-sight (LOS) strategy has been implemented on ROSS for different geometrical patterns of mission tracks. ROSS was then used at sea where it executed a square maneuver while measuring surface chlorophyll. A discussion on the future use of ASV robot systems for multipoint data sampling in coastal areas and its application to CALVAL sites for ocean color remote sensing and in several other areas concludes this paper.

II. Mechanical Design of ROSS

A cross-sectional view of an experimental ASV version of ROSS is drawn in Fig. 3. The hull is a free flooding high-density polyethylene (HDPE) cylinder sliced in two halves to produce two open shells. The nose section of ROSS is a modified reducer section commonly used in agricultural irrigation equipment. This is mirror-welded to the lower half HDPE shell and affords sufficient nose volume to accommodate a miniature *in situ* chlorophyll sensor. The HDPE shells enclose a cylindrical HDPE battery bin containing a bank of 18 lithium polymer cells, and a polyvinyl chloride (PVC) casing that

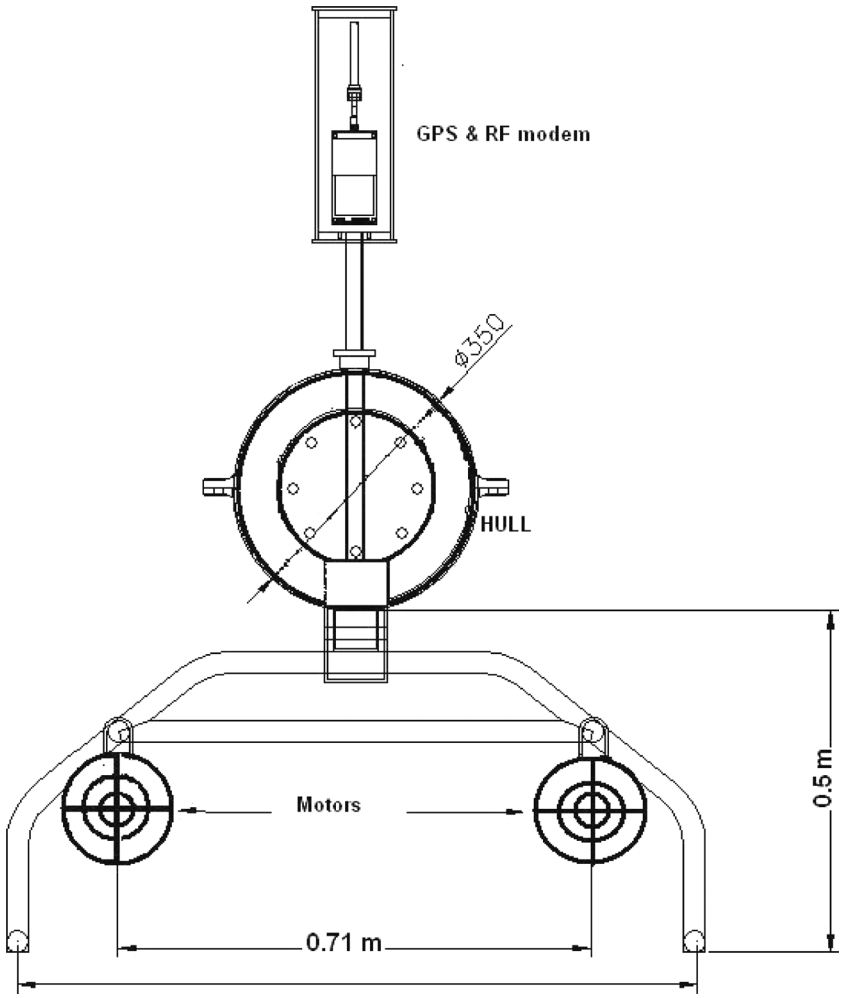

Fig. 2. Cross-sectional view of ROSS showing removable motor frame with dual motors attached to the underside of HDPE hull cover.

accommodates the electronics, embedded controllers, and the inertial measurement unit (IMU) as seen in the longitudinal section of Fig. 3. Each bin has O-ring seals on the face of the endcaps to prevent the entry of water into these bins. A short vertically oriented PVC cylinder which houses the GPS and RF modem electronics, and their antennas is mounted near the nose end of the hull (see Figs. 1 and 2). It is the only part of the sea skimmer that protrudes above the water line. The skimmer is propelled by two brushless dc motors fixed on a detachable aluminum framework attached longitudinally to a welded rib on the lower HDPE shell as in Figs. 1 and 2. The total weight of the sea skimmer in air averages 95 kg. When placed in water, the entire bulk of ROSS is 95% submerged below the sea surface, thus minimizing its profile to surface wind forces, reducing pitching motion from waves, and showing excellent wave transparency particularly in rough weather. Streamlining of the body structure could significantly reduce viscous drag forces when it moves in the water.

A. *Specifications of ROSS*

1) Hydrostatic Considerations: ROSS was designed to be positively buoyant, with principal buoyancy contributions from the battery bin and the electronics casing providing a total buoyancy of 108 kg to offset the total dead weight in air of 95.5 kg. For the purpose of locating the positions of the center of buoyancy (CB) and the center of gravity (CG) of the complete structure, the origin of the reference axes was located at the nose tip. Computations on AutoCAD™ show that the separation between CB and CG in the vertical plane (ZY) is about 51 mm with CG coordinates (Xg, Zg) at (1112, -24) mm and CB coordinates (Xb, Zb) at (1210, $+27$) mm. The hydrostatic restoring moment prevents ROSS from rolling over under most conditions. As a safety measure, two slim line empty PVC floats were secured to the sides of the main hull to reduce roll and pitch to within $\pm 1^{\circ}$. This was not used in all our tests, but if integrated with the main hull, it results in a highly stable platform.

2) Towing Resistance, Propulsion, and Endurance: At a typical forward speed of $v = 1.4$ m/s, which was captured from GPS field data, and an associated Reynolds' number $\mathrm{Re} = 2.45 \times 10^6$, the towing resistance R (or axial drag) of ROSS can be estimated from $R = 0.5\rho \mathrm{ACd}v^2$ to be $\sim$40 N where $\rho = 1000$ kg/m^3 is the density of seawater and $\mathrm{Cd} = 0.4$ is the drag coefficient of the hull taken to be a finite cylinder with fineness ratio $\sim$5. The hull is attached to a motor frame which presents an additional estimated drag of 8 N, resulting in an approximate

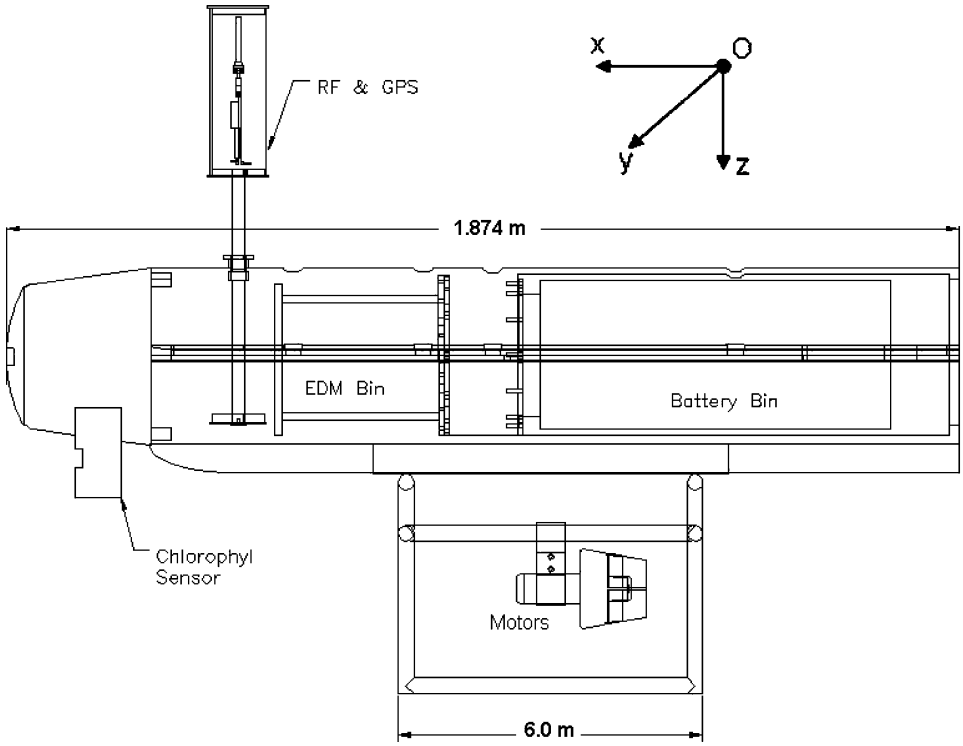

Fig. 3. Longitudinal sectional view of ROSS hull showing placement of battery bin and electronics casing, chlorophyll sensor in nose area, and a vertically oriented tube that houses the radio modem (RF) and GPS antennas. This tube has to protrude out of the sea surface to receive or transmit signals.

total towing resistance of 48 N and a towing power $\mathrm{Pt} = R \times v$ equal to 66 W.

The vehicle is propelled by two Tecnadyne 520 brushless dc motors each capable of a maximum forward thrust of ~70 N at 940 r/min in water. In practice, input power of 304 W was supplied to the thrusters from a bank of lithium polymer batteries at a working current of 1.4 A per thruster. This gives a total propulsion system efficiency $\eta = 0.21$. The endurance of ROSS is approximately 7 h assuming that the 12-Ah bank of batteries is derated by 20%, and that the thrusters require an average current drain of 1.4 A. The hotel payloads on ROSS, which include navigational and communications hardware, chlorophyll, altimeter sensors, and control electronics, have a current drain of <1.5 A from a separate bank with a similar discharge rate of 0.1 C (C-rate). The specifications of the experimental ROSS craft are summarized in Table I.

TABLE I
MAIN SPECIFICATIONS OF THE ROSS VEHICLE

Vehicle parameter	Value
Length , Diameter	1.84 m, 0.36 m
Motor spacing on frame	0.70 m
Total weight in air	95.5 kg
Total buoyancy	108 kg
Z- Separation of (CG -CB)	51 mm
Total drag	48 N
Total thrust	140 N
Propulsion Efficiency @1.4 m/s	0.21
Power source	Li Polymer 18 cells (7.4 V, 12 Ah)
Endurance	~ 7 h @ 1.5 A

III. *In Situ* CALIBRATION OF CHLOROPHYLL SENSOR

A low-cost miniature submersible fluorometer (MiniTracker II, Chelsea Instruments, U.K.) was used in experiments to measure *in situ* chlorophyll concentrations along the mission tracks followed by ROSS. The fluorometer has a concentration range from 0.03 to 100 mg/m^3 which varies linearly with output voltage in the range 0 to 4 V dc . It uses a high-intensity blue (430 nm) light-emitting diode (LED) source as the excitation source and receives fluorescence from chlorophyll cells at a center wavelength of 685 nm. The *in situ* sensor is mounted below the nose volume on ROSS, thus avoiding spurious signals arising from air bubbles released from the turbulent wake of the propeller motors which are located further down in the aft section. The motion of the craft causes seawater to flow past an open cowled enclosure on the sensor endcap. This arrangement emulates a dark chamber and does not require seawater to be pumped through it.

The recommended method of calibrating chlorophyll sensors is by the *in vivo* chlorophyll method. The reason for this is because the calibration graph depends on the plankton species in seawater. For this determination, a Perspex box $(1' \times 1' \times 2')$ was filled with 3 L of freshly filtered seawater whose concentration was measured previously by the standard method using a Turner Design fluorometer [see (1)]. Measurements of the sensor output were made over a longer 15-s interval for different seawater samples, including a blank sample using distilled water. The *in vivo* graph shows a slope of 5.084 mg/m^3/V with a fitted linear regression line to measured chlorophyll concentration of *in situ*

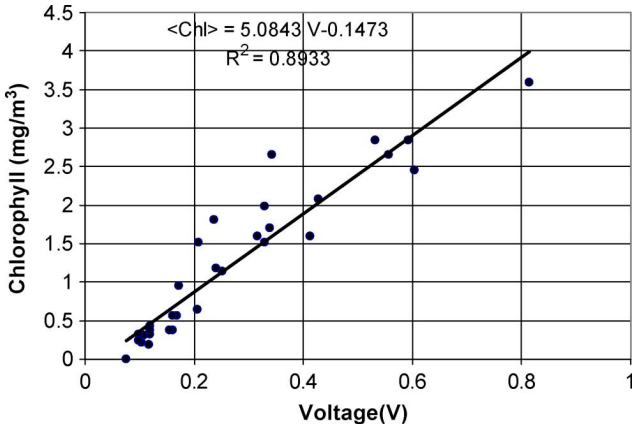

Fig. 4. *In situ* calibration graph of chlorophyll fluorometer sensor output (in volts) against measured chlorophyll concentration (in milligrams per cubic meter) of *in situ* seawater samples collected from different cruises in coastal waters.

water samples in Fig. 4. We took adequate care in suspending the sensor inside the Perspex box of seawater, and in lining the sides of the box with black paper so as to cut down on possible spurious reflection and fluorescence from Perspex. The calibration equation used in converting sensor volts to chlorophyll is

$$\langle \text{Chl}{-}a \rangle = (5.084) \times \text{sensor volts} - 0.147$$

IV. Distributed CAN Networks on ROSS

Two options of either using a centralized or distributed scheme were considered when designing the software and hardware architectures of ROSS. The centralized design is simpler but lacks modularity, and usually involves more powerful hardware which is capable of performing tasks at high speeds, reliably and with support for multithreading or multiprocessing program execution. In a distributed design processing scheme, power can be lower since various smaller and dedicated processors handle smaller and dedicated tasks. This obviously results in dependence upon one or more means of communication networks between these distributed computers or nodes in the system. Hence, a proper choice of a reliable network is very essential. Several distributed networks, namely, Ethernet, RS-422, and CAN, were compared with the underlying consideration that the use of a network should allow relatively easy interfaces with low-cost microcontrollers. Without going into the comparison of networks, we settled for the CAN 2.0-B standard as being a viable option for a modular ASV architecture. CAN networks have been tested extensively in industrial environments and are a well-proven technology that is widely used in the automobile industry [5]. CAN offers the following properties:

1) network nodes allow modular expansion and redundancy of hardware if needed;
2) simplicity in debugging software;
3) prioritization of messages;
4) guarantee of latency times;
5) multicast reception with time synchronization;
6) system wide data consistency;
7) multimaster configurations possible;
8) error detection and error signaling;
9) automatic retransmission of corrupted messages as soon as the bus is idle again;
10) distinction between temporary errors and permanent failures of nodes and autonomous switching off of defect nodes.

The small-message-based protocol is ideal for communication between nodes in the ASV since all control messages required for it are smaller than 8 B. Multicast messages with time synchronization enable multiple nodes receiving consistent data simultaneously. A reliable method of arbitration ensures that important messages take control of the bus. Moreover, nodes that are unreliable are automatically put off the CAN bus. A block diagram of the architecture adopted is shown in Fig. 5.

A. Network Nodes for High- and Low-Level Tasks on ROSS

High-level tasks relating to MC and the acquisition of scientific data are performed by the rabbit core microcontroller (RCM-3110 and RCM 2300) nodes, respectively, on the CAN bus. The RCM 3110 MC node services the navigation sensor suite, GPS receiver for satellite position fixes, and the ultrahigh-frequency (UHF) radio link between the user and the ROSS vehicle (see Fig. 5). The navigation sensor suite consists of an integrated motion and attitude sensing unit (AHRS 400 from Crossbow Technology Inc., San Jose, CA). The AHRS uses three-axes rate gyros, three-axes accelerometers, and a three-axes magnetometer that gives true magnetic heading.

The science node consists of an RCM-2300 module with an eight-channel, 12-b analog-to-digital converter (ADC) integrated circuit (IC) and an additional flash memory of 512 kB flash. It is directly interfaced as shown in Fig. 3 with the chlorophyll and altimeter, and has a 9600-b/s RS-232 serial link to the MC node. The science node also receives GPS-stamps every second if a GPS fix is available to store data in its onboard flash memory.

Low-level tasks on ROSS relating to thruster control and battery monitoring are supervised by three PIC-based nodes which communicate with the MC node via the CAN bus, as shown in the Fig. 5. The thrust on the two motors on the ROSS undercarriage is responsible for maneuvering the vehicle and for propelling it in the surge direction. In addition to these two thruster nodes, there is a PIC-based battery monitoring node. The battery monitoring node measures voltages, current, and energy content in the battery banks. More nodes can be added if required.

V. Communications on the ROSS Vehicle

Communications with ROSS from shore (or ship) are enabled through a high-speed modem (2.4 GHz at 115 kBd) which is interfaced through an RS-232 serial port on a user laptop computer. The graphical user interface (GUI) interface on the laptop acts as the master and has been designed to send commands and to receive data from ROSS (see Section VI). An identical slave modem which is interfaced to a very-high-frequency (VHF) serial port on the MC node resides onboard ROSS.

The frame format adopted for communications between the MC node on ROSS and the ship-based laptop computer is shown in the table at the bottom of the next page.

Two buffers of memory size 270 B each have been allocated in the random access memory (RAM) of the RCM in the MC

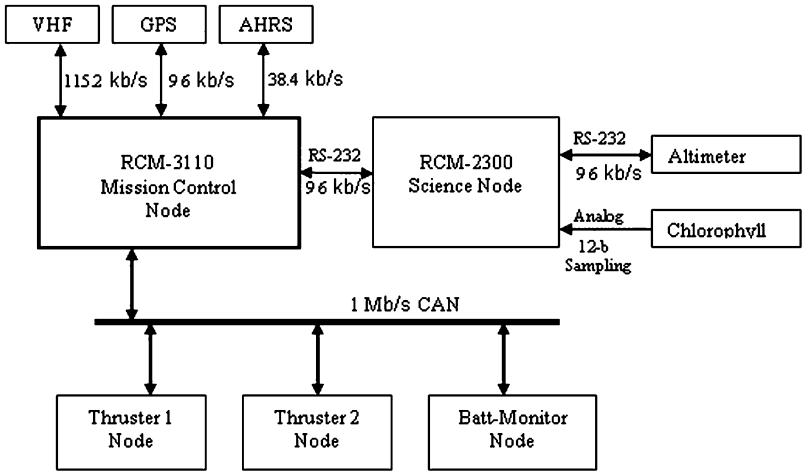

Fig. 5. CAN-based electronics architecture on the ROSS showing high-level nodes for MC and science payloads and low-level nodes that command the two thrusters and monitor power levels of lithium polymer battery banks.

node on ROSS. One buffer is reserved exclusively for "transmit" function and the second buffer is reserved exclusively for "receive" function. These buffers are used for the purpose of constructing transmit and receive frames, respectively.

Start of frame (SOF) contains unique 1-B codes to distinguish between a receiving frame (B3) from the computer to ROSS or a transmitting frame (e.g., A3) from itself (ROSS) to the computer. These codes are known to devices at either end of the communications channel. The advantage of this protocol is that a receiving device rejects any frame that does not begin with one of these valid SOF codes, thus eliminating incomplete or unwanted frames. When a valid frame is received, the next 3 B, i.e., frame ID and frame length are stored in the receive buffer. The frame ID is an identifier, which prescribes the type of frame being communicated (e.g., set thruster voltages, status frame from MC, download page from MC, etc.). The frame length indicates the number of message/data bytes being communicated. These bytes can be anything between 0 and 264 in the present case. The information obtained from the frame length field enables the receiving device to establish the additional number of bytes that are needed to complete construction of the entire frame. After the entire frame (message/data) has been assembled in the buffer of the receiving device, it performs a 16-b cyclic redundancy check (CRC-16) on the data by comparing the computed CRC with that which is present at the end of the frame. If the frame is valid, the receiving device acknowledges it, whereas if the frame is invalid, the receiving device requests for a retransmission of the frame. In this paper, there is also a timeout of 500 ms on the reception of the entire frame. This procedure ensures that the receiving device can recover from conditions where the transmitting device may not send the rest of the frame after sending a valid SOF, ID, and length of frame. In such a case, the MC node flushes its receive buffer and awaits the reception of new messages. The communication protocol described previously has been tested on the ASV using a VHF modem operating at 115 kb/s and has worked satisfactorily within a range of up to 5 km with both devices within line of sight (LOS).

VI. ROSS MC Program

ROSS can be controlled and programmed to follow a mission track using a GUI program which runs on a laptop interfaced to an RF modem. The software has been written for use on a Windows-based PC using Visual C++. It has easy-to-use buttons and allows the operator to configure the ASV in various modes of operation namely in open-loop mode without control, in autopilot control mode of the heading angle, or in GPS guidance mode with autopilot control. The operator is able to script and edit a mission file having selected waypoints specified by latitude and longitude coordinates. The mission tracks are defined by connecting different waypoints in succession. The mission file is uploaded over the RF link to the waiting ROSS for execution by the MC node (see Section IV-A). The software is used to log selected time stamped variables of attitude, GPS fixes, heading and battery voltage in its memory, which can be offloaded for analysis after a mission is completed. The program maintains a periodic check on important vehicle parameters which are updated every second in its display area. If ROSS loses radio contact with this program for more than 10 s, it is programmed to halt the mission and attempt to regain radio contact. Compass calibration can also be performed, which is usually recommended as soon as the vehicle has been deployed to ensure optimum performance from the magnetic compass as it is used in heading control of the vehicle.

VII. Heading Controller of ROSS

In general, the development of a control system starts with an accurate model of the device being controlled. In the case of

SOF (1 B)	Frame ID (1 B)	Frame Length (2 B)	Data bytes (0–264 B)	CRC-CCIT (2 B)

ROSS, this would mean the measurement of the hydrodynamic derivatives of ROSS in a tow tank facility to arrive at a suitable model. This approach is time consuming and expensive. Given the expected simplicity of the final model, we adopted an input–output identification method that relies on free open-loop maneuvers and is based on the following simple realistic observations.

- The symmetry of the ROSS implies that its surge motion can be decoupled from sway and yaw [6].
- ROSS has a widebeam of 70 cm with spaced out dual motors and an inherent restoring couple that aligns the vehicle vertically to the sea surface. The couple works to oppose the reactive hydrodynamic roll caused by motor torques [7]. The effect is amplified at higher speeds when ROSS tends to heel outwards on a turn. As observed in Section II, the dynamics associated with roll and pitch motion can be made negligible by attaching two slim line floats on either side of the main hull. For simplicity, the heave motion component is not considered but would be important in the presence of sea surface waves.

Based on the previous observations, we assume a linear maneuvering model and a proportional-derivative (PD) autopilot for yaw control. The linear model relates the yaw rate r to the differential torque τ imparted by propellers. Let $r(s)$ and $\tau(s)$ be Laplace transforms of r and τ, respectively. The Nomoto linear model adopted [6], which is velocity dependent, yields the transfer function

$$\frac{r(s)}{\tau(s)} = \frac{K(1+T_3 s)}{(1+T_1 s)(1+T_2 s)} \tag{1}$$

where K is a gain and $T_{i=1,2,3}$ are time constants that can be determined from the yaw rate data collected in a standard turning circle ship maneuver as proposed by the International Towing Tank Conference (ITTC) [6]. Physical considerations on the stability of surface vehicles [7] suggest that the second-order Nomoto model predicts a real zero and two real poles. We will verify this inference by fitting the model to field data as given in the following.

The turning circle maneuver is a test that can be used to find the steady turning radius of the vehicle and to check how well the dual thrusters respond to differential step control voltage changes, and the resultant changes it produces on the vehicle's heading and performance in motion. The test was performed without disturbance in a large swimming pool by applying a 3.5-V differential step voltage having an equivalent differential thrust of ∼12 N to the thrusters. The vehicle responds by moving in a circle at a constant yaw rate of ∼8.5°/s and a continuous change in heading in the range 0°–360°. The diameter of the turning circle ∼5 m of ROSS is shown in Fig. 6 as an XY plot using GPS fix data. This gives a constant turning speed of 0.38 m/s.

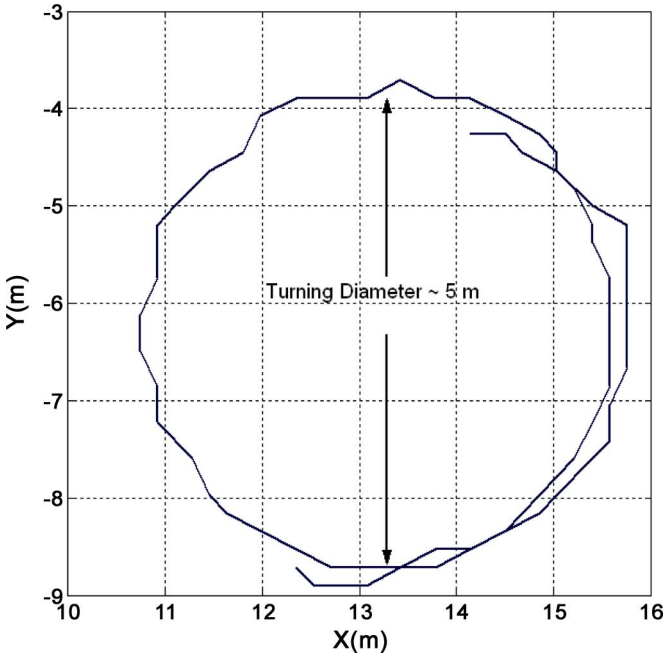

Fig. 6. Turning radius (∼2.5 m) of ROSS at low speed of 0.4 m/s is used in deriving the vehicle model.

A. Estimating the Vehicle Model From Open-Loop Step Response

The data set used in the estimation of vehicle model for ROSS corresponds to the turning circle data. The low differential step response in open loop ensured that the system was operated within the bounds of a linear model. The measured yaw rate output in degrees per second from the AHRS rate gyro is shown plotted against time in Fig. 7 over a span of 35 s to ensure that the yaw rate had settled to a steady-state value of ∼8.5°/s. The method of Franklin *et al.* [8] was used in estimating the transfer function from the time response to a step input, by assuming the fact that the response is a sum of exponentials of the form

$$Y(t) = y(\infty) + Ae^{-\alpha t} + Be^{-\beta t} + Ce^{-\gamma t} + \dots \tag{2}$$

where the parameters can be determined from real data. The data set was first smoothed by using a running average filter over the interval 0–70 s and truncated beyond 35 s. The average over 8–35 s was set equal to $y(\infty)$. Following the procedure in [8], the parameters in (2) were estimated as $\alpha = 0.63$ rad/s, $\beta = 0.53$ rad/s, $A = -1.219$, and $B = 0.212$, from which the Nomoto model

$$\text{TF} = \frac{1.61(s+0.51)}{(s+0.63)(s+0.53)} \tag{3}$$

was obtained. The estimated transfer function (TF) yields a pair of real poles at $s = -0.63$ rad/s and $s = -0.53$ rad/s, and a single zero at $s = -0.51$ rad/s. Notice the almost (stable) pole-zero cancellation, which effectively reduces the order of the TF to one. From the aforementioned, ROSS has an approximate open-loop bandwidth of 0.63 rad/s and a settling time (to step input) of ∼6 s.

B. Simple PD Heading Controller for ROSS

For ROSS, a simple PD control law was adopted. Let ψ and ψ_d be the actual and desired heading, respectively. The PD controller assumes the form

$$\tau = K_p(\psi_d - \psi) - K_d r \tag{4}$$

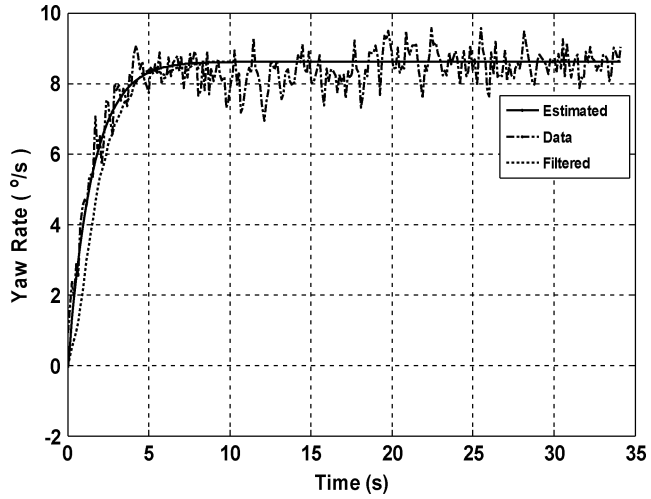

Fig. 7. Filtered and actual yaw rate response (degrees per second) of the ROSS vehicle is plotted as a function of time, and compared with the solid line fit from a second-order Nomoto model.

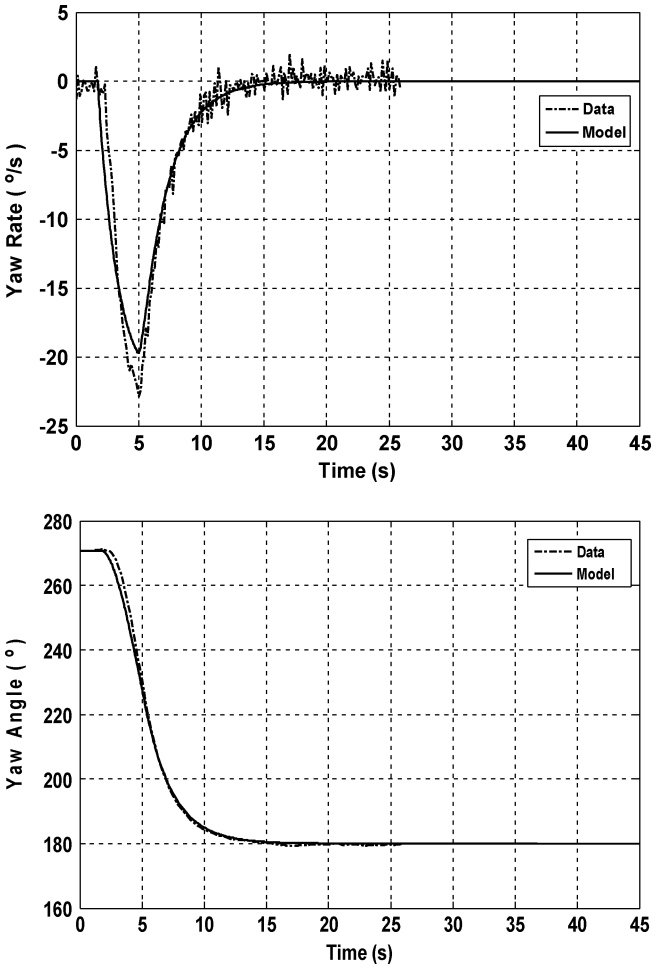

Fig. 8. (a) Heading autopilot response of yaw rate (degrees per second) compared with model output. The yaw rate converges to zero after 15 s. (b) Convergence of ROSS to a set heading angle of 180° compares favorably with model output to within ±2°.

where τ is torque about z-axis, r is yaw rate and K_p and K_d are proportional and derivative gains, respectively. Integral action can be avoided in this case, because the plant naturally offers an integral term that corresponds to the fact that yaw is the integral of yaw rate. The proportional term with gain K_p has the effect of reducing the rise time but increases the overshoot, whereas the derivative term with K_d improves the transient response and decreases the overshoot. In this case, the gains $K_p \sim 0.9$, and $K_d \sim 1.8$ were selected so as to ensure sufficiently fast response to step inputs while keeping the control bandwidth smaller than that of the thrusters. In practice, actual measurements of yaw and yaw rate were obtained from an AHRS unit at the sampling rate of ∼7 Hz.

1) Closed-Loop Control Simulation—Pool Tests: The closed-loop performance of the ROSS heading controller was verified by using the Nomoto model in (3) and control law gains $K_p = 0.9$, and $K_d = 1.8$ in (4).

The time responses of yaw rate and yaw angle to a change of 90° in commanded yaw angle are plotted in Fig. 8(a) and (b), and compared to the corresponding simulated responses derived from the plant model of (3). It is seen that the heading controller was able to converge from initial heading of 270° to 180° within 15 s, at which time the corresponding yaw rate had settled to zero. The gains K_p and K_d derived from the simulation model could be changed "on the fly" over the RF modem link, and this feature in the GUI software helped speed up the tuning controller gains in the field.

VIII. GPS-Assisted Guidance of ROSS

Simple LOS waypoint guidance [10] for ROSS was accomplished by providing a heading angle to the heading controller of ROSS. The heading angle is computed by finding the LOS between the current GPS position of the vehicle and the waypoint to be reached. The cascade configuration of guidance controller as input to the heading controller is shown in Fig. 9. This arrangement separates guidance and autopilot functions given that the waypoints are well spaced, and the response of ROSS under control is sufficiently fast to track the heading command provided by the guidance system at 1 Hz (as determined from GPS fixes every second) [10]. The commanded heading angle (LOS angle) to the horizontal plane of the sea surface is based on the relation

$$\Psi_{\mathrm{LOS}} = \tan^{-1}\left\{\left(Y_k - Y(t)\right) / \left(X_k - X(t)\right)\right\} \qquad (5)$$

where $[X_k, Y_k]$, $k = 1 \ldots, N$, are the coordinates of the N waypoints stored in the vehicle mission script memory, and $[X(t), Y(t)]$ are the GPS coordinates converted into an internal 2-D representation in Cartesian XY frame where the present position of the vehicle is taken as the instantaneous origin of the moving frame of reference. Since it is close to impossible that the vehicle navigates to a waypoint with precision, and since oceanographic applications do not demand this precision, we need to define a "radius of acceptance ρ_o," around the particular waypoint such that when the current radius $\rho(t)$ at time t satisfies

$$\rho^2(t) = \left[X_k - X(t)\right]^2 + \left[Y_k - Y(t)\right]^2 < \rho_o^2 \qquad (6)$$

the next waypoint is selected [6]. If this condition is not met, for whatever reason, e.g., an environmental disturbance, then the

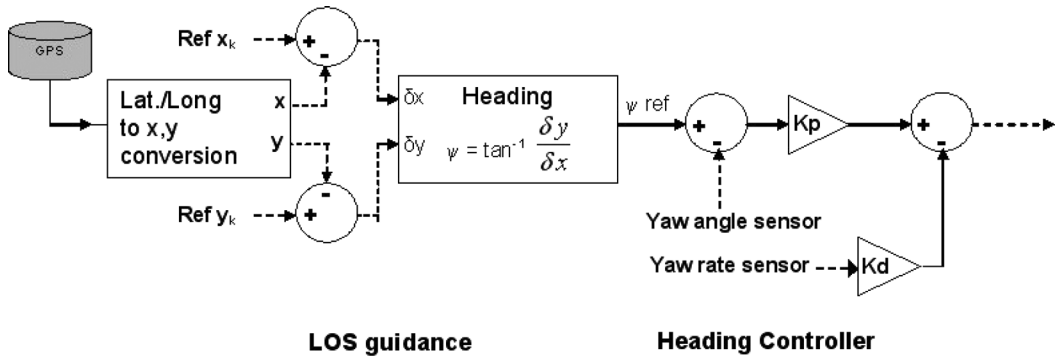

Fig. 9. Cascade configuration of the LOS guidance heading input to heading controller.

guidance algorithm will direct the vehicle to circle the waypoint till criterion (6) is satisfied before triggering the logic to move to the next waypoint.

In spite of its simplicity, the LOS waypoint guidance scheme adopted is perfectly suited for a number of applications where the key requisite is that the vehicle visits a number of selected sites in sequence. In a number of important applications, however, it is required that the vehicle converges to and follows a reference path in the presence of shifting currents and wind, while tracking a desired speed profile (e.g., in bathymetric surveys where adjacent tracks must be followed with great precision). In this case, a path-following algorithm must be implemented onboard the vehicle. The reader will find in [11] a lucid exposition of path-following algorithms using LOS guidance with cross-track error or integral of cross-track error control, where the latter is introduced to combat the effects of a constant cross current. See also [12] and the references therein for a general introduction to the problem of path-following control under a different perspective inspired by the pioneering work for wheeled robots described in [13]. Path-following control laws will be implemented on our ASV and tested in the future.

A. *Examples of LOS Guidance Tracks of ROSS in Sea Tests*

The LOS controller in cascade with the heading controller of Fig. 9 was run on the Simulink toolbox in MATLAB before real field trials in the sea. The GPS sensor was simulated by reverse calculating the X, Y Cartesian coordinates from the heading angle (ψ) and an assumed velocity of ROSS. The simulation was able to handle several known waypoints and at known constant vehicle velocities. We present the following three examples of real field trails at sea near coastal areas off Goa, India: 1) a triangular maneuver close to the shore, 2) classical parallel tracks with six waypoints, and 3) a simple square maneuver but with *in situ* data acquisition from a calibrated chlorophyll sensor described in Section III.

Example 1—Triangular Maneuver: The first example to test the LOS guidance algorithm is shown in Fig. 10(a). The mission track consists of three waypoints configured as a triangle. The simulated mission tracks are drawn in for comparison with the actual tracks executed by ROSS (as a solid line). Interestingly, the vehicle overshot waypoint 3, circled around it, recovered, and proceeded towards the starting waypoint 1. A maximum

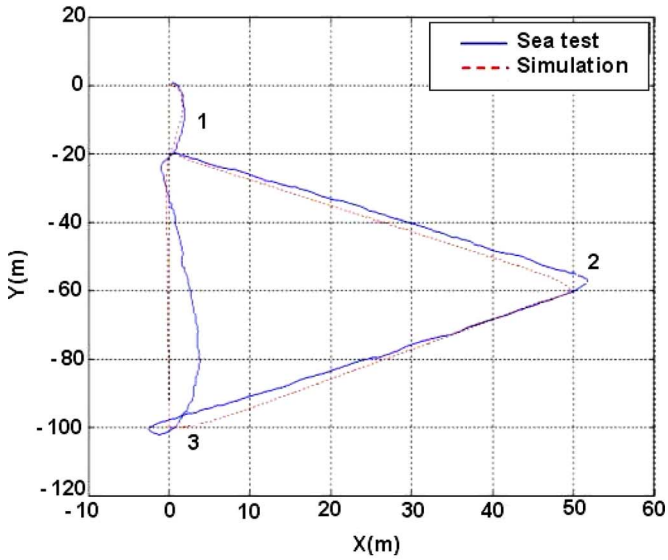

(a)

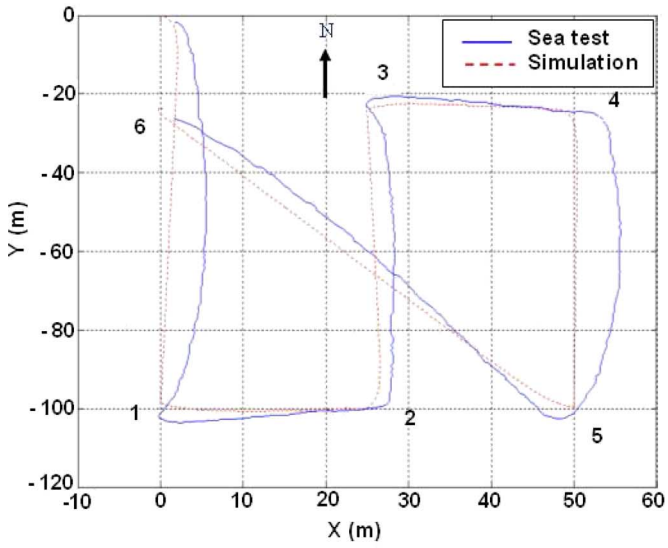

(b)

Fig. 10. (a) Comparison of simulated and actual path followed by ROSS in the triangular maneuver. The acceptance radius was set to 1 m (typical value should be twice the length of a vehicle). (b) Comparison of simulated and actual path followed by ROSS for the parallel track pattern in shore area site.

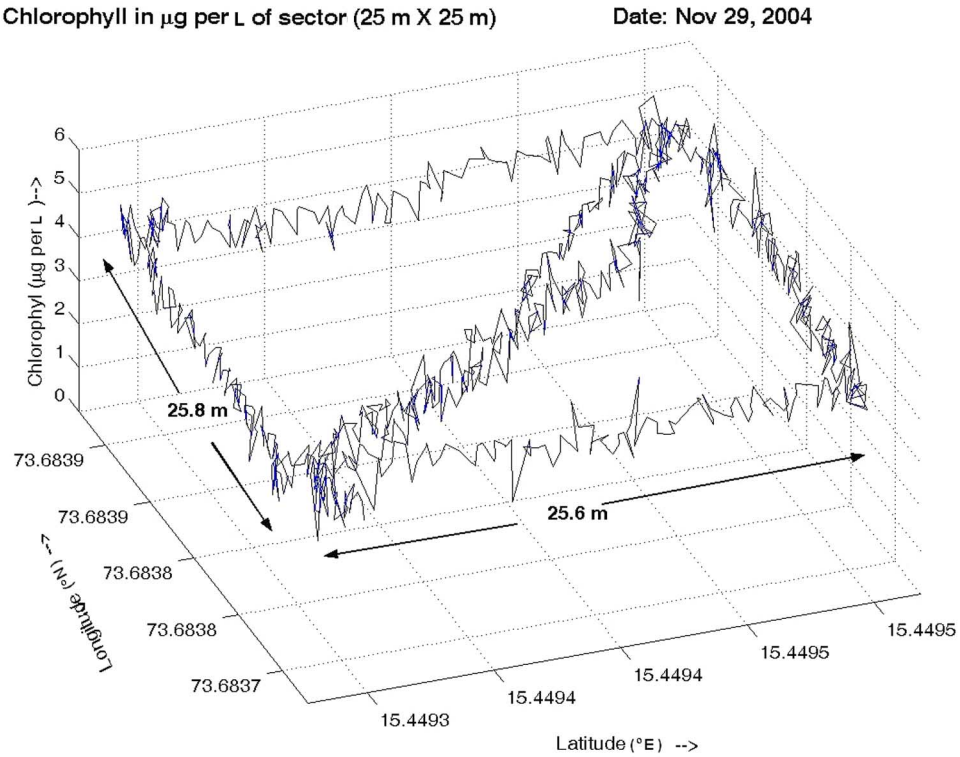

Fig. 11. Surface chlorophyll distribution obtained along the tracks of square maneuver at sea. Each point on the surface corresponds to a value of chlorophyll concentration in milligrams per cubic meter identified in position by the latitude and longitude coordinates.

deviation of 3.6 m was observed on the leg between waypoints 3 and 1 due to the effect of a shore current which curved the track.

Example 2—Parallel Tracks: The parallel track pattern shown in Fig. 10(b) is a standard track set used in most bathymetric surveys. Here, we used six waypoints to define the configuration. The actual tracks of the ROSS craft are shown as solid lines compared to the simulated mission tracks as dotted lines. The maximum deviation of the actual from the simulated is 5 m. We observe the effect of current disturbances on the tracks showing that the simple LOS waypoint guidance implementation used here does not necessarily yield a straight line between the waypoints. To achieve this, more sophisticated path-following control laws are required [11].

Example 3—GPS-Tagged Chlorophyll Measured Along a Square Track: In this example, the calibrated Minitracker II *in situ* chlorophyll sensor which was described in Section III was fitted below the front nose of ROSS. The output of the chlorophyll sensor data was sampled and digitized by the RCM 2300 controller of the science node, time stamped, and GPS tagged with latitude and longitude coordinates. The result is plotted as a surface chlorophyll distribution in Fig. 11. Although the plotted sample area of 25 m $\times$ 25 m is small, it illustrates the potential of using an ASV craft with well-calibrated optical and acoustic sensors to map ocean surface and seabed properties at high resolution. The variability of chlorophyll is clearly exposed here, and indicates a new way of looking at the surface variability of chlorophyll that could not be possible using a satellite or a ship. If the larger areas are mapped with surface ASV, we can begin to unfold the valleys and crests in the distribution of chlorophyll and compare this with real measurements by satellites around a CALVAL site.

IX. Conclusion

This paper provided a detailed description of the engineering design and implementation of a simple low-cost ASV that uses GPS-assisted waypoint guidance. An RF modem link permits the user to monitor the ASV during its mission, and to download data, or to stop and start the vehicle over the RF link. The electronics is based on inexpensive CAN network nodes which simplifies the hardware and software of the vehicle, and makes it possible to incorporate scientific sensors to measure surface ocean properties. Most oceanographic studies do not demand high precision in latitude and longitude position coordinates, which would otherwise be necessary in bathymetric surveys where DGPS systems are used to obtain centimeter level precision in position. The main application here would be to monitor changes or trace trends in surface oceanographic parameters on a seasonal basis over kilometer areas. In this development, a single fluorometer was used to measure surface chlorophyll while the ASV moves along mission tracks. However, this approach can be extended in the future to include spectroradiometers to measure upward radiance and downward irradiance, absorption and attenuation meters on the ASV to provide useful high-resolution data sets that complement what is measured on a CALVAL buoy over a single pixel. Calculation shows that if the estimated 7-h endurance of ROSS is fully utilized then a sample area of 2.5 km $\times$ 2.5 km comprising $\sim$50 satellite ground pixels of the OCEANSAT 1 could be covered in that time.

Coastal bathymetric surveys by ASV platforms could be refined in accuracy by correcting them with DGPS references and real-time tidal data from a nearby tide station transmitting such data to the ASV in real time during a mission. This has implications in the design of early warning systems to monitor storm surge and tsunamis, and also as input data to the mathematical modeling of such events.

The potential of ASV as robot platforms for monitoring the coastal zone needs hardly to be stressed as the issue of sustainability of coastal ecosystems gains world wide recognition. It is surprising that simple ASV such as that described here has not received the same interest as its better known cousin—the autonomous underwater vehicle (AUV). With further innovations on the payloads and motors, the ASV can be fabricated at a cost low enough to be used in large numbers by coastal states.

ACKNOWLEDGMENT

The authors would like to thank the Director of the National Institute of Oceanography, Goa, India, for extending the use of facilities.

REFERENCES

[1] J. Woods, "Ocean predictability," in *Anton Bruun Memorial Lecture*. Paris, France: IOC, UNESCO, 1999, p. 30.
[2] ASIMOV Team, "Robotic ocean vehicles for marine science applications: The European ASIMOV project," in *Proc. MTS/IEEE OCEANS*, RI, Sep. 11–14, 2000, vol. 1, pp. 409–415.
[3] J. E. Manley, A. Marsh, W. Cornforth, and C. Wiseman, "Evolution of the autonomous surface craft AutoCat," in *Proc. MTS/IEEE OCEANS*, 2000, vol. 1, pp. 403–408.
[4] A. Mascarenhas, R. Madhan, E. S. Desa, E. Desa, and F. D'Souza, "Remotely operable sea skimmer," in *Proc. Mar. Technol. Soc. Annu. Conf./Ocean Community Conf.*, 1998, pp. 740–744.
[5] *"CAN Specification 2.0,"* Robert Bosch GmbH, 1991, Stuttgart, Germany.
[6] T. I. Fossen, *Guidance and Control of Ocean Vehicles*. New York: Wiley, 1994, pp. 168–174.
[7] M. A. Abkowitz, "Stability and motion control of ocean vehicles," MIT, Cambridge, MA, NSF Sea Grant Project GH-1, 1969.
[8] G. F. Franklin, J. D. Powell, and A. Emami-Naeini, *Feedback Control of Dynamic Systems*, 4th ed. Upper Saddle River, NJ: Pearson Education, Inc., 2002, pp. 173–179.
[9] N. S. Nise, *Control Systems Engineering*, 3rd ed. New York: Wiley, 2000, p. 351.
[10] A. J. Healey and D. Lienard, "Multivariable sliding mode control for autonomous diving and steering of unmanned underwater vehicles," *IEEE J. Ocean. Eng.*, vol. 18, no. 3, pp. 327–339, Jul. 1993.
[11] A. Healey, "Guidance laws, obstacle avoidance and artificial potential functions," in *Advances in Unmanned Marine Vehicles*, ser. IEE Control Series 69, G. Roberts and R. Sutton, Eds. London, U.K.: Institution of Engineering and Technology, 2006, ch. 3, pp. 43–46.
[12] A. Pascoal, C. Silvestre, and P. Oliveira, "Vehicle and mission control of single and multiple autonomous marine robots," in *Advances in Unmanned Marine Vehicles*, ser. IEE Control Series 69, G. Roberts and R. Sutton, Eds. London, U.K.: Institution of Engineering and Technology, 2006, ch. 17, pp. 353–386.
[13] C. Samson, "Path following and time-varying feedback stabilization of a wheeled mobile robot," in *Proc. Int. Conf. Control, Autom., Robot. Vis. (ICARCV)*, Singapore, 1992, pp. RO.13.1.1–RO.13.1.5.

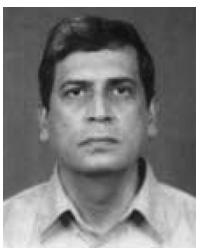

Elgar Desa (M'06) was born in Kolkata, India, in 1951. He received the B.Sc. and Ph.D. degrees in physics from the Kings College, University of London, London, U.K., in 1973 and 1976, respectively.

Currently, he is a Scientist at the Marine Instrumentation Division, National Institute of Oceanography, Goa, India.

Pramod Kumar Maurya was born in Gorakhpur, India, in 1977. He received the M.S. degree in electronic science from Devi Ahilya University, Indore, India, in 1999.

He has worked as a Research Fellow in Aeronautical Development Agency, Bangalore, India, for Light Combat Aircraft program of India. Currently, he is a Scientist at the Marine Instrumentation Division, National Institute of Oceanography, Goa, India.

Arvind Pereira was born in Goa, India, in 1980. He received the B.E. degree in electronics and communications from the Gogte Institute of Technology, Belgaum, Karnataka, India, in 2002. Currently, he is working towards the M.S. degree in electronics engineering at the University of Southern California, Los Angeles.

He has worked as a Fellow and Project Assistant at the National Institute of Oceanography, Goa, India.

António M. Pascoal received the Licenciatura degree in electrical engineering from the Instituto Superior Técnico (IST), Lisbon, Portugal, in 1974 and the M.S. degree in electrical engineering and the Ph.D. degree in control science from the University of Minnesota, Minneapolis, in 1985 and 1987, respectively.

Currently, he is an Associate Professor of Control and Robotics at ISR-IST.

R. G. Prabhudesai received the M.Sc. degree in physics and electronics from Karnataka University, Karnataka, India, in 1975.

Currently, he is a Scientist at the National Institute of Oceanography, Goa, India.

Antonio Mascarenhas received the M.E. degree in industrial engineering from Bombay University, Bombay, India, in 1975.

Currently, he is a Scientist at the National Institute of Oceanography, Goa, India.

Ehrlich Desa received the Ph.D. degree in electronics and electrical engineering from the University of Sheffield, Sheffield, U.K., in 1972.

He served as a Director of the National Institute of Oceanography, Goa, India. Currently, he is the Head of the Section Capacity Building at IOC UNESCO, Paris, France.

R. Madhan received the B.Tech. degree in electrical engineering from Regional Engineering College, Calicut, India, and the M.Tech. degree in power and energy systems from Regional Engineering College, Surathkal, India, in 1990 and 1998, respectively.

Currently, he is a Scientist in Marine Instrumentation Division, National Institute of Oceanography, Goa, India.

S. G. P. Matondkar received the Ph.D. degree in applied biology from Goa University, Goa, India, in 1987.

He is a Biological Oceanographer at the National Institute of Oceanography, Goa, India.

Gajanan Navelkar received the M.Tech. degree in digital electronics from the Regional Engineering College, Surathkal, India, in 1998.

Currently, he is a Scientist at the National Institute of Oceanography, Goa, India.

Shivanand Prabhudesai received the Diploma in mechanical engineering from the Government Polytechnic, Goa, India, in 1993.

Currently, he is a Technical Assistant at the Marine Instrumentation Division, National Institute of Oceanography, Goa, India.

Sanjeev Afzulpurkar received the M.S. degree in applied electronics from the Osmania University, Hyderabad, India, in 1981.

Currently, he is a Scientist at the National Institute of Oceanography, Goa, India.